A novel nonintrusive method to resolve the thermal dome effect of pyranometers: Radiometric calibration and implications

Q. Ji,[1,2] S.-C. Tsay,[2] K. M. Lau,[2] R. A. Hansell,[1,2] J. J. Butler,[2] and J. W. Cooper[2,3]

Received 26 June 2011; revised 30 September 2011; accepted 16 October 2011; published 17 December 2011.

[1] Traditionally the calibration equation for pyranometers assumes that the measured solar irradiance is solely proportional to the thermopile's output voltage; therefore, only a single calibration factor is derived. This causes additional measurement uncertainties because it does not capture sufficient information to correctly account for a pyranometer's thermal effect. In our updated calibration equation, temperatures from the pyranometer's dome and case are incorporated to describe the instrument's thermal behavior, and a new set of calibration constants are determined, thereby reducing measurement uncertainties. In this paper, we demonstrate why a pyranometer's uncertainty using the traditional calibration equation is always larger than a few percent, but with the new approach can become much less than 1% after the thermal issue is resolved. The highlighted calibration results are based on NIST traceable light sources under controlled laboratory conditions. The significance of the new approach lends itself to not only avoiding the uncertainty caused by a pyranometer's thermal effect but also the opportunity to better isolate and characterize other instrumental artifacts, such as angular response and nonlinearity of the thermopile, to further reduce additional uncertainties. We also discuss some of the implications, including an example of how the thermal issue can potentially impact climate studies by evaluating aerosol's direct radiative effect using field measurements with and without considering the pyranometer's thermal effect. The results of radiative transfer model simulation show that a pyranometer's thermal effect on solar irradiance measurements at the surface can be translated into a significant alteration of the calculated distribution of solar energy inside the column atmosphere.

Citation: Ji, Q., S.-C. Tsay, K. M. Lau, R. A. Hansell, J. J. Butler, and J. W. Cooper (2011), A novel nonintrusive method to resolve the thermal dome effect of pyranometers: Radiometric calibration and implications, *J. Geophys. Res.*, *116*, D24105, doi:10.1029/2011JD016466.

1. Introduction

[2] The measurements of solar irradiance over the globe play an important role in climate studies because solar radiation is the primary driving force of climate. Pyranometers are used worldwide to measure solar irradiance. Traditionally, the uncertainty of a high-quality pyranometer is greater than a few percent, which is not desired for studying long-term climate change. For example, the radiative forcing due to doubling the amount of CO_2 in the atmosphere is $\sim$4 W m^{-2} [*Ad Hoc Study Group on Carbon Dioxide and Climate*, 1979], and the global average of radiative forcing for different agents and mechanisms is around a couple of W m^{-2} [*Pachauri and Reisinger*, 2007]. However, a $\pm$ 2% uncertainty (specifications of pyranometer) [e.g., *World Meteorological Organization* (*WMO*), 2008] on the $\sim$184 W m^{-2} ($\sim$263 W m^{-2} if cloud free) global annual mean solar radiation at the Earth's surface [*Trenberth et al.*, 2009] is over $\pm$ 3.6 W m^{-2}, comparable to or larger than the expected ranges of the climate change signals. A reduced uncertainty in pyranometer measurements will have profound implications, such as gaining the ability to better discern the radiative forcing, or the global dimming and brightening [*Wild*, 2009]. Furthermore, a more accurate data set of solar irradiance will also help improve the evaluation of the effects of clouds and aerosols on climate studies. An example of the latter effect is explored later in the paper.

[3] A pyranometer's larger than 2%$\sim$3% uncertainty [*WMO*, 2008] is related to its thermal dome effect (TDE), which traditionally is not quantified. Shading a pyranometer can help reveal and infer its thermal effect [e.g., *Gulbrandsen*, 1978]; however, it does not provide a direct nonintrusive measurement of TDE. In addition, any object casting the shade also imposes its own contribution dynamically to the thermal environment. This situation has changed since the studies that explicitly describe the TDE [e.g., *Bush et al.*, 2000; *Ji and Tsay*, 2000; *Haeffelin et al.*,

[1]ESSIC, University of Maryland, College Park, Maryland, USA.
[2]Earth Sciences Division, NASA Goddard Space Flight Center, Greenbelt, Maryland, USA.
[3]Sigma Space Corporation, Greenbelt, Maryland, USA.

Copyright 2011 by the American Geophysical Union.
0148-0227/11/2011JD016466

2001; *Dutton et al.*, 2001]. Continuing the effort to directly addressing the thermal issue, *Ji and Tsay* [2010] have introduced an innovative nonintrusive method that enables a reliable and routine monitoring of TDE; thus this thermal effect of pyranometer can be correctly accounted for in measurements of solar irradiance.

[4] Historically, the measured solar irradiance, I, is regarded as being simply proportional to the output voltage of the pyranometer's thermopile, V:

$$I = c_{\mathrm{h}} V, \tag{1}$$

where c_{h} is an empirical calibration factor. Regardless of how c_{h} is determined, this traditional calibration equation carries a large uncertainty because it is incapable of fully capturing the dynamic thermal behavior of the pyranometer. To reduce the uncertainty, we have derived a new calibration equation:

$$I = c\,V + f\,\sigma\left(T_s^{\,4} - T_d^{\,4}\right), \tag{2}$$

where T_s is the temperature of the receiving surface of the thermopile, and T_d is the effective dome temperature. In addition, $\sigma = 5.67 \times 10^{-8}$ J s^{-1} m^{-2} K^{-4} is the Stefan–Boltzmann constant; and the intrinsic calibration constants c and f are stable physical properties [*Ji and Tsay*, 2000]. f is also called the "dome factor," a quantity related to the dome emissivity and the geometry of a pyranometer (discussed in this paper). Furthermore, because the thermopile's output is referenced to the temperature of the pyranometer's case (i.e., T_c), T_s can be determined by $T_s = T_c + \alpha V$, where α is a thermopile parameter, and we regarded it as a constant in our previous study [*Ji and Tsay*, 2010]. A schematic of a pyranometer illustrating a couple of our nonintrusive methods for deriving T_d is described in Appendix A.

[5] The difference between the traditional and the new calibration equations is obvious. The former has one measurement (i.e., V) and a single empirical factor (i.e., c_{h}), unable to properly represent the TDE; while the latter incorporates three measurements (i.e., V, T_c, and T_d) and four true physical constants (i.e., c, f, σ, and α), able to quantify the TDE by the temperature-related term. A variety of methods for calibrating pyranometers are listed in WMO's Guide to Meteorological Instruments and Methods of Observations [*WMO*, 2008, chapter 7.3.1]. Since they all depend on equation (1), we refer this type of calibration as a V1C1 calibration; standing for one measured variable, and one constant to be determined. For example, whenever a single calibration constant is provided by a manufacture or a research laboratory such as Broadband Outdoor Radiometer Calibrations (BORCAL at the National Renewable Energy Laboratory, available at http://www.nrel.gov/aim/borcal.html), it is a V1C1 calibration. Under this convention a method using equation (2) becomes a V3C4 calibration. However, because σ is an universal constant, and following our previous studies we assume α is a know constant, we are effectively dealing with a V3C2 calibration in this study. Additionally, our new method is backward compatible, because the V1C1 calibration remains intact and available.

[6] A characteristic listed in the specification of a pyranometer [*WMO*, 2008] is its "zero offset," but how it affects the uncertainty of a pyranometer is not specified. In order to correct the offset errors in measurements of diffuse solar irradiance, *Dutton et al.* [2001] developed a data correction procedure where the correction factor is derived from the output of a collocated pyrgeometer that measures atmospheric infrared irradiance. This is an indirect approach involving multiple instruments. These results are useful if the diffuse component is required when calibrating total irradiance radiometers by reference to a standard pyrheliometer and a shaded reference pyranometer [*International Organization for Standards*, 1993]. The method is expensive if used in the routine measurement of total irradiance because it requires a pyrheliometer for the direct solar component, a shaded pyranometer for the diffuse sky component, and a shaded pyrgeometer for the thermal correction of the shaded pyranometer. In addition, all three instruments must be mounted on a solar tracker; and the pyranometer and pyrgeometer need to be ventilated. Another complication is related to the pyrheliometer being subject to thermal effects (discussed in this paper). In contrast, our new method eliminates the "zero offset" directly from a pyranometer [*Ji and Tsay*, 2010].

[7] Different design and make of pyranometers are available commercially. Their response to thermal effect are different too [e.g., *Michalsky et al.*, 2003]. We focused on Epply Precision Spectral Pyranometer (PSP) (available at http://www.eppleylab.com), because its design has remained relatively unchanged for decades; therefore, there are relatively longer records of consistent measurement, which is useful for climate change studies. Nevertheless, our new method and discussions are not limited to PSP, we expect them to be also valuable in improving other instruments and measurements.

[8] This paper is structured as follows. In section 2 we present our method for radiometric calibration of a pyranometer against a calibrated NIST-traceable light source. In section 3 we show the measurement results illustrating the weakness of the V1C1 calibration and the advantage of the V3C2 one. In section 4 we discuss implications of this new approach, including some of the knowledge gained, followed by an example of model simulation demonstrating the potential impact of TDE on climate studies. Finally, the conclusion and future work are presented in section 5.

2. Radiometric Calibration

[9] In this study, integrating spheres maintained in a clean room of the Radiometric Calibration Facility at NASA Goddard Space Flight Center (available at http://spectral.gsfc.nasa.gov) are used as references to examine both the traditional and new calibration equations. Figure 1a illustrates a PSP mounted in front of an integrating sphere. This light source is calibrated by comparison with NIST-calibrated standard irradiance lamps using monochromators [*Walker et al.*, 1991]. Its spectral radiance is shown in Figure 1b.

[10] The calibration procedure is straightforward: for V1C1, a calibration factor is determined by $c_{\mathrm{h}} = \{I/V\}$ for equation (1); for V3C2, c and f can be derived as the intercept and slope of a linear fit from $\{I/V\} = c + f\{\sigma(T_s^4 - T_d^4)/V\}$ for equation (2). In addition, although T_d is not directly measured, it can be verified under special conditions from T_c by

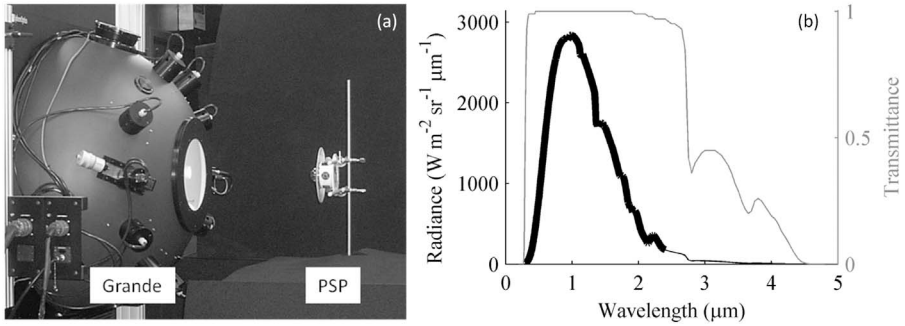

Figure 1. (a) Grande is a 1 m Teflon integrating sphere with an aperture of 25.40 cm in diameter. It has 9 independently controlled lamps for producing different levels of radiance. A PSP can be mounted with the thermopile facing the aperture. (b) The irradiance from Grande is determined by a combination of its spectral radiance, viewing geometry, and spectral cut-off of PSP's dome. The gray curve illustrates a transmittance for WG295 glass. The thick curve highlights the currently NIST-traceable part of spectral radiance (i.e., between 0.4 and 2.4 μm).

maintaining a pyranometer in the dark until a thermal equilibrium state is achieved (i.e., $V = 0$ and $T_d = T_c$).

[11] Note that the parameter space over which the overall calibration uncertainty of a pyranometer can be adequately quantified is a much bigger question to tackle. To properly address this question will require the collective efforts of the scientific community as a whole whereby the current methodology can be fully tested in different environments under different situations. Here we regard a light source as an absolute radiometric reference for showing how V1C1 and V3C2 track a reference, thereby demonstrating why measurements can be improved.

3. Results

[12] Eight rounds of calibration are depicted in Figure 2 as an example to illustrate the effects of TDE. The measured temperatures are shown in Figure 2a, where T_s and T_c are plotted as the thin curves at the top and on the bottom,

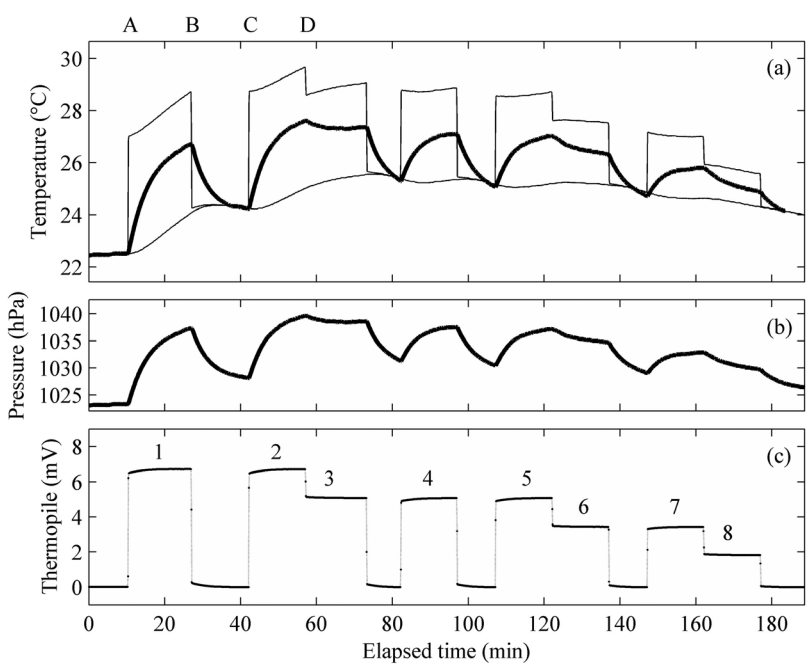

Figure 2. Example of eight rounds of calibration which took about 3 h. (a) The light is turned on at point A, making all the measured temperatures in a PSP to increase (see section 3). The light is blocked at point B about 15 min later, causing the temperatures to decrease and approach each other. The thermal equilibrium is reached after several minutes. The light is turned on again at point C, followed by a reduction of the light intensity at point D. The similar pattern is repeated in the later rounds. (b) The pressure in the sealed volume between domes (compare Appendix A). (c) The varying output voltage of thermopile. See section 3 for details.

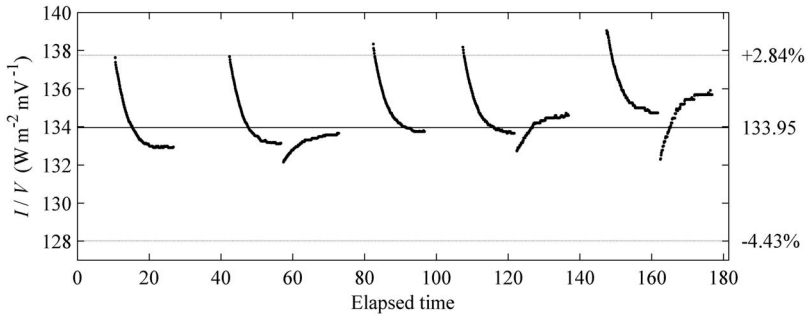

Figure 3. The I/V is the calibration factor that should be a constant according to the traditional calibration equation. For example, it should remain at 133.95 W m^{-2} mV^{-1} according to a BORCAL result, marked by the solid line. In reality I/V varies with temperature across a wide range as shown in the thick curve. See section 3.1 for details.

respectively. In the middle is T_d shown as the bold curve, which is proportional to the pressure of the air sealed between the domes as plotted in Figure 2b.

[13] This example reveals that T_s responds immediately when a PSP is exposed to light, while T_d changes slowly and T_c lags further behind. Naturally, in response to the "solar heating," the larger the thermal mass is, the smaller the rate of change will be. When it is blocked from light, T_s approaches T_c promptly while all the temperatures decrease, and the thermal gradient diminishes after several minutes. Once exposed to light the second time, all temperatures start to rise again, but begin with a higher value due to the heating in the previous round, and will reach higher levels. Notice that if we just reduce the intensity of light instead of fully blocking it to return the PSP to dark conditions, then T_d will decrease, but other temperatures may still be increasing with smaller rates under the reduced heating than in the previous round; however, all temperatures start to decrease if the irradiance is further reduced to a point that the heating became insufficient. In this example the irradiance was set to 879.6 W m^{-2} in rounds 1 and 2, then reduced to 668.3 W m^{-2} in rounds 3 to 5, and further reduced to 455.2 W m^{-2} in rounds 6 and 7, and finally to 244.3 W m^{-2} in round 8. Generally the system warms up in the early rounds when irradiance is larger and cools down later when irradiance becomes smaller, which to a certain extent represents morning and afternoon conditions, respectively.

[14] It is important to point out that in each round of calibration the output voltage of the thermopile varies noticeably and does not reach a stable value for a prolonged period of time while the variation of the light source is negligible (less than 0.1%), as illustrated in Figure 2c. The changing output voltage is cause by the TDE. In this example the transitional period lasted about 10 min in the first round when the temperature swing was relatively large. The thermal gradient inside the PSP diminishes faster in the later rounds when the irradiance is smaller.

3.1. V1C1 Calibration

[15] The limitation of a V1C1 calibration is demonstrated in Figure 3, where the curve shows the calibration factor (i.e., I/V, or c_h). Evidently, c_h neither starts at a fixed value nor reaches a fixed one in each round of calibration. This is unwanted for equation (1), because it may make a PSP's thermopile seemingly nonlinear against temperature. However, it is expected according to equation (2), which predicts that if I remains stable, then the larger the TDE, the smaller the V, and vice versa.

[16] Also marked in Figure 3 is a V1C1 calibration from BORCAL (i.e., c_h = 133.95 W m^{-2} mV^{-1}, +2.84%, −4.43%, for PSP#33109F3). Notice its large uncertainty range, which is typical in a V1C1 method related to the lack of an accurate interpretation of the thermal effect. To correct the errors in the V1C1 calibrated measurements, a correction method such as the one developed by *Dutton et al.* [2001] is needed.

3.2. V3C2 Calibration

[17] The potential of using the V3C2 calibration equation is demonstrated in Figure 4a, where the calibration constants (i.e., mean value ± standard deviation) are based on four rounds of calibration; two each at I = 879.6 and 668.3 W m^{-2}. Notice that the linearity of the curve is an indication on how well equation (2) can capture the reality. To show repeatability, Figure 4b overlays twelve more rounds that include I = 455.2, 244.3, also 960.3, 729.7, 497.0, and 266.7 W m^{-2}; realized by turning on different lamps in the integrating sphere, and by altering the distance between the PSP and the integrating sphere. In this particular example, the I/V versus $\sigma(T_s^4 - T_d^4)/V$ curve shifted slightly during those extra rounds when irradiances were smaller; however, the slope (i.e., f) remains relatively unchanged after a shift, which is consistent with f being a stable factor independent of the uncertainty in I and c. We found that the shift does not diminish when the PSP's "thermopile temperature compensation circuit" is disabled, indicating that it is not caused by the slight drift of temperature during these particular rounds. The shift can be caused by several reasons, such as biases in I, nonlinearity in V, or error in T_d. Future work is necessary to resolve the issue to further reduce the uncertainty.

[18] In order to determine T_d, we sealed the space between the inner and outer domes of a PSP to create a constant volume gas thermometer [*Ji and Tsay*, 2010]. This method is nonintrusive because it does not block the field of view of thermopile; however, it modifies a PSP slightly. To evaluate whether this modification impacts the performance of the PSP, we tested one of our alternative methods that does not

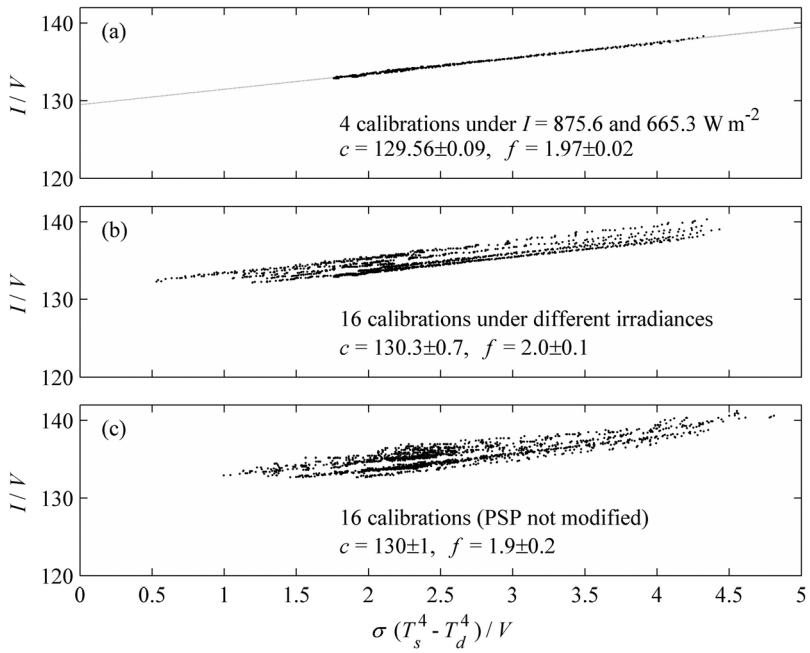

Figure 4. Example of the new calibration. (a) A consistent result from selected rounds. (b) Result including additional rounds. (c) Same as Figure 4a but without modification to the PSP (compare Appendix A). See section 3.2 for details.

require such modification (see Appendix A). Although this alternative method is less straightforward in determining T_d, and produces slightly more noise in the calibration results as shown in Figure 4c, it indicates that a PSP's performance remains consistent regardless of modification.

3.3. Contrast Between the Two Results

[19] An example of comparing the V1C1 and the V3C2 calibrations is given in Figure 5. When exposed to a known irradiance of 893.7 W m^{-2}, the V1C1 result reached

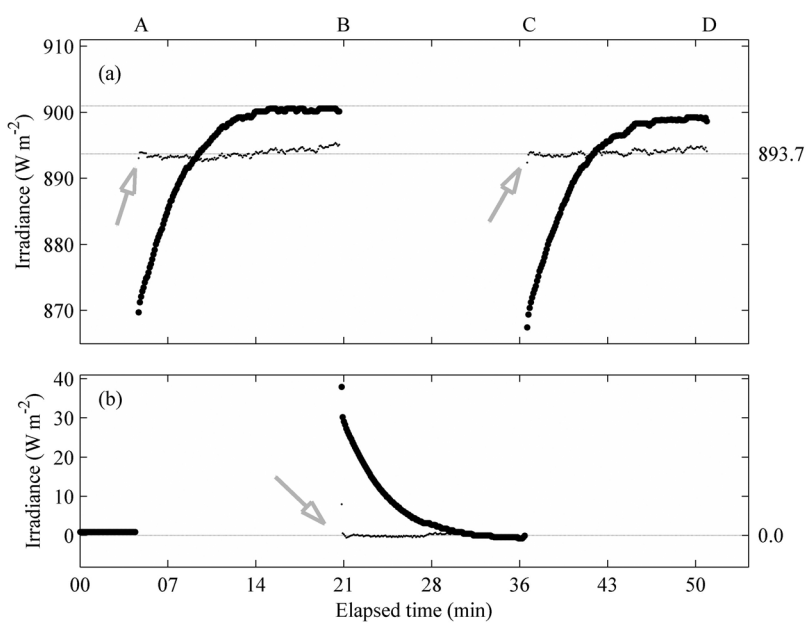

Figure 5. The traditional (thick curve) versus the new (thin curve) calibration results. The sampling rate is about every 5 s. The PSP is exposed to light at point A, then blocked from light at point B, and exposed to light again at point C. The arrows highlight that the new calibration tracks the correct irradiance promptly. (a) Notice that the traditional result is slightly different in period C to D from the result in period A to B. (b) The prolonged nonzero results of the traditional calibration in dark conditions. See section 3.3 for details.

Table 1. Sample Calibration Results of a PSP Using Different Types of Domes

Type of Dome	f	c (W m^{-2} mV^{-1})
WG295 #1	1.5	130
WG295 #2[a]	1.5	130
GG395 (yellow dome)[a]	1.5	124
RG695 (red dome)[a]	1.8	128
WG295 #3[b]	1.5	130
Quartz[c]	1.3	129
WG295 #4[d]	1.6	132
WG295 #4[e]	1.7	133
WG295 #5[f]	2.0	130.3
WG295 #5[g]	1.9	130

[a]Same inner dome as in WG295 #1.
[b]A different set of inner and outer domes.
[c]The transmittance is assumed to be 100% between 0.2 and 3.5 μm, 0% elsewhere.
[d]Yet another set of inner and outer domes; mounted on a brass collar for testing.
[e]Same as above except sealed.
[f]One more set of sealed inner and outer domes.
[g]Same as above, except unsealed.

870 W m^{-2} initially, then drifted to 901 W m^{-2} in about 10 min. Once repeated in the next round, it approached a couple of W m^{-2} lower, corresponding to about 1°C rise in temperature. In contrast, the result from the V3C2 calibration started to track the known irradiance within a few seconds every time. Figure 5b highlights a situation when light was blocked. After an initial drop, it took over 10 min for the V1C1 calibrated result to decrease from about 30 to 0 W m^{-2}, while the V3C2 calibrated result promptly jumped to 0 W m^{-2}. The high precision of the new calibration is evident.

[20] According to the WMO specification, the response time of a high-quality pyranometer is less than 15 s. This is based on using a V1C1 calibration for the measurement to reach 95% of final value. In contrast, it will reach 99.9% of final value within 15 s in a V3C2 calibration. More importantly, the results from equation (2) will remain consistent when the calibration is repeated, which reflects that because c and f represent stable physical properties their values can be more accurately determined over time with better statistics. This is unachievable in a V1C1 calibration, because the empirical factor in equation (1) depends on environmental conditions and does not converge to a constant.

4. Implications

[21] There are many important implications in realizing that a pyranometer can have a much smaller uncertainty once its thermal effect is accounted for. For example, we used to assign each PSP to a specific ventilator hoping the set would maintain a consistent thermal characteristic. We also tried to use reversed ventilation to reduce the thermal effect. With the new calibration, ventilation is rendered noncritical concerning the thermal effect. This makes it easy for us to deploy a solar-powered network of PSPs and to generate a more consistent data set, in light of that a consistent global data set is of importance for climate studies. A few other things we have learned are briefly highlighted in the following.

4.1. Different Domes and Dome Factors

[22] We tested several "clear domes" (WG295 glass, available at http://schottglass.com) on the same PSP, and found that they yield a consistent result using the new calibration. Other than WG295, we also use "color domes," such as GG395, for selecting spectral bands from 0.4 to 3 μm and RG695 for 0.7 to 3 μm. Traditionally a PSP is calibrated with a clear dome; and when a color dome is needed for quantifying the energy partitioning in solar irradiance, an empirical scale factor is applied. It is difficult to determine and to justify a scale factor without knowing the TDE.

[23] With equation (2), we treat all types of domes equally except when considering the corresponding spectral transmittance in the determination of the irradiance from the light source. We found that an RG695's TDE changes faster and varies over a larger range but can balance at a smaller value than a WG295's. It is because an RG695 dome absorbs more solar radiation than a WG295 dome does; therefore, its T_d becomes closer to T_s than with a WG295 dome. The resulting distinct thermal behavior indicates that a scale factor is not appropriate for an RG695 in terms of a highly accurate and consistent measurement.

[24] As listed in Table 1, an RG695 dome has a slightly larger dome factor than a WG295 dome, which in turn has a slightly larger dome factor than a quartz dome (i.e., 1.8 versus 1.5 versus 1.3 for PSP#33109F3). In theory, for an idealized pyranometer whose thermopile's receiving surface occupies the whole area underneath the dome, its dome factor is the emissivity of dome which is smaller than 1.0 [*Ji and Tsay*, 2000]. In reality, the receiving surface in a PSP only covers a small fraction of the area, allowing its surroundings to contribute noticeably to TDE, leading to a larger "effective value" of f. It may be improved in the future with a better calibration equation.

4.2. Essence of Thermal Effect

[25] To truly understand TDE it is important to realize that the thermal effect is not limited to a PSP-like pyranometer. Generally speaking, there will be "TDE" as long as the detector senses any blockages thermally in its field of view. A blockage can be a dome or a collimator and so on. An Eppley Normal Incidence Pyrheliometer (NIP) is an example: without a large thermal mass, a NIP can approach thermal equilibrium more easily than a PSP does, therefore displays a smaller "nighttime offset"; however, the sunlight or a sudden change of air temperature can cause a large thermal gradient along the cylinder of a NIP, introducing a significant thermal effect.

[26] Figure 6a shows the output of a NIP during four rounds of tests when it is alternatively exposed and blocked from the NIST-traceable light source. Similar to a PSP, after an initial quick response to the change of light, the output of the NIP starts to drift slowly depending on temperature and its gradient in the instrument. As long as the temperature changes, the NIP's output will drift and balance to a different value. In dark conditions, the "nighttime offset" can be either positive or negative, depending on the relative temperature between the front and back ends of the NIP. Note that in the fourth round when the irradiance was reduced, the temperature which was measured near the window of the NIP became lower too; and it dropped several degrees of

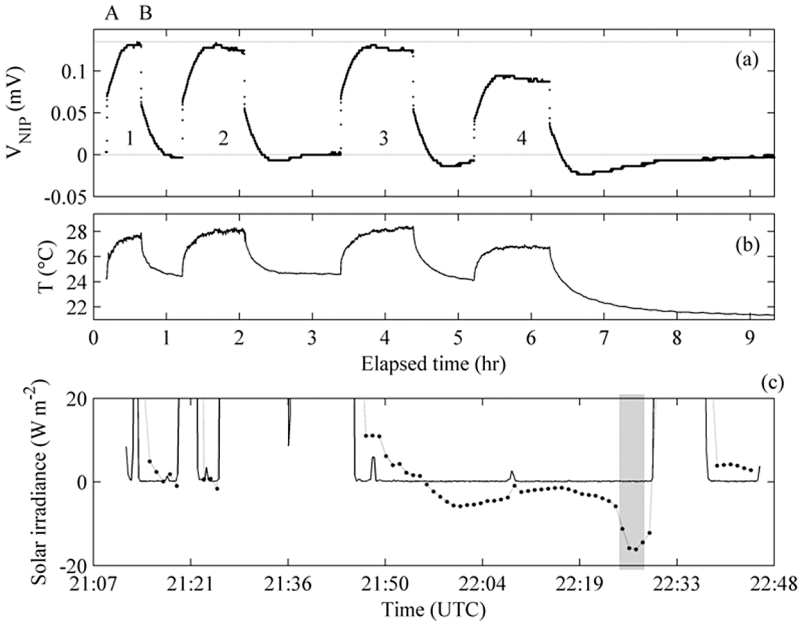

Figure 6. Thermal behavior of NIP. (a) In round 1 the light was turned on at point A; and after rose from 0 to ~0.074 mV swiftly, the output voltage of the NIP, V_{NIP}, drifted slowly up to ~0.13 mV in about half an hour. At point B the light is blocked; and V_{NIP} dropped halfway to ~0.06 mV quickly, then started to drift toward 0 mV slowly. This was repeated three more rounds with V_{NIP} reached slightly different values depending on the environmental temperature. In round 4 the light intensity was set to 75% of that in the previous rounds. (b) The temperature, *T*, increased when the light was on, and decreased when the light was blocked. (c) An example showing about an hour and half of data in the late afternoon on 9 May 2003. The solid curve is for a TDE-free ASD spectroradiometer, and the dotted curve is for a NIP. There was a rain shower during the shaded period. See section 4.2 for details.

Celsius further in the dark during the last few hours, as shown in Figure 6b. Notice the corresponding drift of the "nighttime offset" shown in Figure 6a.

[27] Figure 6c demonstrates the NIP's thermal effect in field measurements. This particular example is from the 2003 ARM Aerosol IOP (Atmospheric Radiation Measurement Aerosol Intensive Observation Period), when we used an ASD spectroradiometer with its appropriate foreoptics (available at http://www.asdi.com) to measure the direct solar irradiance side-by-side with a NIP. It shows that when the direct solar beam is blocked by clouds, the output of a TDE-free instrument responds promptly; while the result of a TDE-laden NIP always lags behind, and can drift to negative values due to the thermal effect depending on environmental conditions. Figure 6c also illustrates a special condition when the output of the NIP dropped below -16 W m^{-2} responding to a dramatic change in temperature caused by a short passing rain shower that started around 2225 UTC on 9 May 2003 and lasted a few minutes. This example clearly differentiates between surface measurements of instruments that are free of the thermal effect or not.

[28] This leads to why we derived a smaller *f* value in our previous study [*Ji and Tsay*, 2010], where we explored using the combined data from a NIP and a shaded PSP as a reference to demonstrate a calibration procedure. The reason is that the reference is not TDE-free; for example, if TDE exists on both sides of equation (2) and their values are identical, then the derived *f* will erroneously become zero in a calibration. It also explains why involving a TDE-laden instrument does not yield an ideal calibration reference.

4.3. Impact on Climate Studies

[29] In this section we consider derivation of an aerosol's direct radiative effect (DRE) as an example to show the potential impact of a pyranometer's thermal issues on climate studies. It is based on over two months (April–June 2008) of ground-based observations in a remote semiarid desert region frequented by dust outbreaks and local pollution during springtime in northwestern China. Explicitly, with or without accounting for TDE, the measured downward solar irradiance on the surface will be different which directly impacts the energy balance. Implicitly, in order to simulate these different versions of measurement using a radiative transfer model (RTM), some assumptions in the RTM such as the type of aerosol must be adjusted accordingly. In turn, the modeling results will be altered, including DRE, throughout the column of atmosphere. A brief description of the RTM and the relevant measurements are given in Appendix B.

[30] In this case study, a set of traditionally calibrated PSP data can be well simulated by using an aerosol model of pure dust in the RTM. However, the observed aerosols contain soot emitted from local sources [*Li et al.*, 2010]. This brings a scenario that when soot is added into the aerosol model while all other assumptions in the RTM remain the same, the simulated downward solar irradiance on the surface will

decrease, matching the TDE corrected measurements. Based on ~1,700 available data points, our calculation shows that when soot contributes ~1.7% of optical thickness, the irradiance decreases ~3 W m^{-2} on average. This alters the aerosol's DRE from −57 to −59 W m^{-2} (−2 W m^{-2}, or +4% relative difference) on the surface; from 48 to 52 W m^{-2} (4 W m^{-2}, or +8%) inside the column atmosphere; and from 9 to 7 W m^{-2} (−2 W m^{-2}, or −20%) at the top of the atmosphere. Of course, this is just one possible scenario, but it demonstrates that treating TDE differently can lead to significant differences in model simulations, and thus altering the interpretation of the radiative impact over the column atmosphere.

5. Conclusion and Future Work

[31] Using a highly stable light source in the laboratory, we have illustrated the limitation of the traditional V1C1 (one variable/measurement, one constant/calibration coefficient) calibration, and demonstrated that a pyranometer can track a reference with high precision in a new V3C2 calibration with the thermal effect addressed. This can facilitate the quest to reduce pyranometer's measurement uncertainty from over a few percent to less than 1%, which is critical for climate studies. We have also highlighted some important implications of this study, which included taking a pyrheliometer as an example to show that the thermal effect is not limited to a pyranometer. An application of how the thermal issue can potentially impact climate studies was also investigated by evaluating a direct radiative effect of aerosol using field measurements with and without considering the pyranometer's thermal effect. Results showed that model simulations of atmospheric radiative transfer are significantly altered by not accounting for such effects. In short, an improved pyranometer with the thermal issue resolved will have a higher precession and accuracy to help produce a more consistent data set that can play an important role in studies of climate change.

[32] Although the potential of an improved pyranometer has been demonstrated under controlled laboratory conditions, there are many aspects to be further explored. These include, but are not limited to, how representative the indoor calibration at room temperature is, how the thermal expansion of a pyranometer's case and domes contributes to measurement uncertainty, and how viewing the light source sideways affects the thermal gradient in PSP. Some of these issues may be secondary, because the new calibration equation relies on stable physical properties that are less temperature sensitive. More importantly, the cosine response is convolved with the thermal effect when the traditional calibration is used; while they can be separated in laboratory measurements once the new calibration is applied. A better understanding of the cosine response will help improve the calibration and its application to field measurements.

[33] Additionally, it is critical to correct historical data sets for climate studies. Although a data set can never be fully corrected without accurate TDE information, we have found that certain auxiliary measurements may be good surrogates for establishing a reasonable correction, including the temperature from a collocated pyrgeometer, or the air temperature adjacent to the pyranometer [*Ji and Tsay*, 2010]. With time, the new method can be refined to help improve solar irradiance measurements and ultimately climate studies.

Appendix A: Two Methods for Measuring a Pyranometer's Effective Dome Temperature

[34] While its case temperature, T_c, can be captured directly by putting a thermistor inside a pyranometer, its effective dome temperature, T_d, cannot be as easily measured. In a method illustrated in Figure A1, the space between a PSP's domes can be converted into a constant-volume gas thermometer [*Ji and Tsay*, 2010]; therefore, T_d is derived from a pressure measurement by applying the ideal gas law. Figure A1 also depicts an alternative method that still relies on a pressure measurement and the ideal gas law, but does not require any modification to the instrument other than adding a thermistor and attaching a barometer to the case of a pyranometer. Here we summarize how these methods work. For a sealed volume (Figure A1a), the ideal gas law states that

$$T_d = P_d/r, \tag{A1}$$

where P_d is the pressure measured by a barometer, and r is a constant proportional to the density of the trapped air between the domes. r can be determined under dark conditions when the thermal gradient diminished (i.e., where $V = 0$ and $T_d = T_c$ thus $r = P_d/T_d = P_d/T_c$). Alternatively, the attached barometer is for capturing the air pressure, P, inside the whole instrument (Figure A1b). For simplification, we assume that T_d and T_c represent the temperatures above and beneath the receiving surface of thermopile, respectively. According to the ideal gas law, when the pyranometer reaches thermal equilibrium at a given temperature T_0 (i.e., $T_d = T_c = T_0$), the pressure inside the instrument will be

$$P_0 = \frac{m_d + m_c}{v_d + v_c} T_0, \tag{A2}$$

where m_d and m_c are proportional to the masses of air occupying the volume above the thermopile (i.e., v_d), and elsewhere inside the case (i.e., v_c), respectively. Normally, $T_d \neq T_c$ and $P \neq P_0$ without thermal equilibrium; however, P is always the same in both v_d and v_c, therefore simultaneously,

$$P = \frac{m_c}{v_c} T_c, \text{ and } P = \frac{m_d}{v_d} T_d, \tag{A3}$$

Let $q = v_d/(v_c + v_d)$ and using equations (A2) and (A3), we have

$$T_d = \frac{q}{(P_0/T_0)/(P/T_c) - (1 - q)} T_c. \tag{A4}$$

[35] Here P_0/T_0 is proportional to the density of the trapped air inside a pyranometer, and ideally remains a constant if there is no thermal expansion of the instrument or leak of air. In addition, q defines the fraction of the volume above the thermopile over the total volume inside the instrument. We found that the volume between the domes consists of ~13% of the total volume inside a PSP. After compensating for the part between the inner dome and

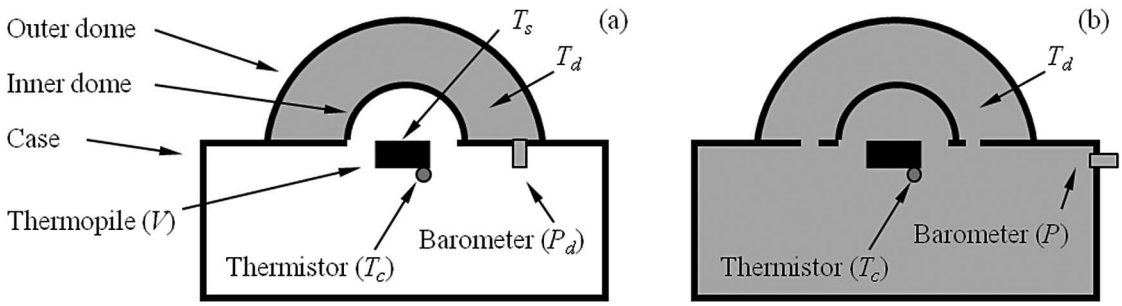

Figure A1. Schematically, a PSP is a thermopile mounted on a metal case and covered by two layers of glass dome. The interior of PSP is isolated from the environment. The thermopile outputs a voltage V. (a) By sealing the space between the two domes and adding measurements of T_c and P_d, we can determine the effective dome temperature, T_d, via equation (A1). In addition, the temperature of the receiving surface of thermopile, T_s, is a function of V and T_c. (b) Without sealing the space between the two domes, T_d can still be determined from T_c and the pressure of the trapped air inside the whole PSP, P, using equation (A4).

thermopile, we derived $q \approx 0.23$. Although q is well defined in geometry, its effective value may vary slightly depending on thermal expansion or other factors, such as which part of air is effectively contributing to T_d. Nevertheless, once P_0/T_0 and q are measured, T_d is determined from T_c and P.

Appendix B: Radiative Transfer Model and Relevant Measurements

[36] A publicly available multiple-scattering plane-parallel RTM has been used for estimating the shortwave (SW) irradiances near the ground surface and at the top of the atmosphere (TOA). The model was developed by Fu-Liou [*Liou et al.*, 1988; *Fu and Liou*, 1993] and later modified and distributed by the NASA Langley group (available at http://snowdog.larc.nasa.gov/rose/fu0602). Originally the SW spectrum in this RTM is divided into 6 bands (0.2–0.7, 0.7–1.3, 1.3–1.9, 1.9–2.5, 2.5–3.5, and 3.5–4.0 μm; with the first band further divided into 10 subbands). In order to be consistent with the measurements, we weight the calculated irradiances in those bands according to the transmittance values for the pyranometer glass dome. The longwave irradiance is also calculated in the model [see *Hansell et al.*, 2010], although the signal-to-noise ratio is much smaller from aerosol such as dust. The major input parameters for the RTM are listed in Table B1, while the minor ones such as trace gases remain at the model"s default values.

[37] The relevant measurements that are used for constraining the RTM are (1) a Cimel sunphotometer (available at http://aeronet.gsfc.nasa.gov) for aerosol optical depth (AOD) at 0.34, 0.38, 0.44, 0.5, 0.67, 0.87, and 1.02 μm, and column precipitable water vapor (PWV); (2) a micropulse lidar (MPL) (available at http://mplnet.gsfc.nasa.gov) for backscatter profile; (3) sounders (available at http://weather.uwyo.edu/upperair/sounding.html) for temperature and relative humidity (average from two closest sites at Jiuquang and Minqin in China); (4) a UV radiometer for column ozone; (5) a ASD spectroradiometer for surface spectral albedo; and (6) PSP pyranometers for downward SW irradiance on the surface. The measurement site is located in a semiarid desert area on a dry riverbed sparsely coved by tumbleweed.

[38] A midlatitude summer atmosphere profile included in the model is regarded as a template and updated with the available sounding data. Subsequently the updated profiles are scaled to match the measured column ozone and PWV amounts. The instantaneous AOD at the seven Cimel wavelengths are distributed proportionally to the normalized relative backscatter observed by the MPL. The model simulation is performed only when a cloud screened Cimel observation is available. All the inputs to the model are linearly interpolated to the time stamp of the Cimel measurements.

Table B1. Major Inputs for the Radiative Transfer Model

Parameter	Source	Comment
Location	Observation	Zhangye Climatological Observatory (~1.5 km above sea level, 100°16.575′E, 39°4.940′N).
Atmospheric profile	Observation and model	Modeled "mid-latitude summer" profile if sounding and other measurements are lacking.
Solar incident angle	Observation	Determined by location and time.
Surface albedo	Observation	Interpolated to the model bands of wavelength.
Aerosol optical depth	Observation	At 7 Sun photometer wavelengths.
Water vapor	Observation and model	Combination of sounding and modeled profile; scaled to match Sun photometer measurement.
Aerosol type	Model	Defined in model. The one most consistent with observations is selected.
Aerosol distribution	Observation and model	Based on the modeled profile; updated according to the MPL backscatter.
Cloud type	Model	Only the cloud-screened conditions are simulated.

[39] Aerosol's shortwave direct radiative effect (DRE) is defined as a perturbation in net irradiance given by the difference between the incoming and outgoing radiative energies caused by aerosols when compared to an aerosol-free reference. In other words, regarding the incoming irradiance (I) is as positive from the perspective of each location, DRE = $\delta I(\tau) - \delta I(0)$; where, at TOA $\delta I_{\mathrm{TOA}} = I^{\uparrow}_{\mathrm{TOA}} - I^{\downarrow}_{\mathrm{TOA}}$, across the column atmosphere $\delta I_{\mathrm{atm}} = I^{\downarrow}_{\mathrm{TOA}} + I^{\uparrow}_{\mathrm{surface}} - I^{\uparrow}_{\mathrm{TOA}} - I^{\downarrow}_{\mathrm{surface}}$, and on the surface $\delta I_{\mathrm{surface}} = I^{\downarrow}_{\mathrm{surface}} - I^{\uparrow}_{\mathrm{surface}}$. Except for an imaginary aerosol-free condition ($\tau = 0$), $\delta I(0)$ is a modeled state with the same atmospheric properties as for $\delta I(\tau)$. Notice that since $\delta I(0)$ does not exist in reality, therefore DRE is not a directly measureable parameter. Our calculated DRE are instantaneous values [e.g., *Haywood et al.*, 2003] based on the time stamp of the Cimel sunphotometer, versus diurnally averaged quantities [e.g., *Anderson et al.*, 2005].

[40] Uncertainties in broadband irradiance measurements can contribute to inaccurate assessments of aerosol's DRE. For example, SW pyranometers can introduce measurement errors due to the instrument's cosine response [e.g., *Collins*, 1966; *Michalsky et al.*, 1995]. In a study of DRE, *Fu et al.* [1999] concluded that discrepancies between modeled and measured irradiance can be largely due to the radiation measurement errors. Other studies [e.g., *McComiskey et al.,* 2008] have also examined the sensitivity of DRE to various model parameters (i.e., aerosol and surface properties, etc); however, the impact of TDE to the determination of DRE has not caught much attention.

[41] **Acknowledgments.** This research is supported by NASA Radiation Science Program, managed by Hal B. Maring. It is also partially supported by the NASA Goddard Space Flight Center's Internal Research and Development. We thank SMARTLabs team for conducting field measurements (see http://smartlabs.gsfc.nasa.gov); CFL team for supporting laboratory calibration (see http://cf.gsfc.nasa.gov); and BORCAL team for providing outdoor calibration (see http://www.nrel.gov/aim/borcal.html).

References

Ad Hoc Study Group on Carbon Dioxide and Climate (1979), *Carbon Dioxide and Climate: A Scientific Assessment*, Natl. Acad. of Sci., Washington, D. C.

Anderson, T. L., et al. (2005), An "A-Train" strategy for quantifying direct aerosol forcing of climate, *Bull. Am. Meteorol. Soc.*, *86*, 1795–1809, doi:10.1175/BAMS-86-12-1795.

Bush, B. C., F. P. J. Valero, and A. S. Simpson (2000), Characterization of thermal effects in pyranometers: A data correction algorithm for improved measurement of surface insolation, *J. Atmos. Oceanic Technol.*, *17*, 165–175, doi:10.1175/1520-0426(2000)017<0165:COTEIP>2.0.CO;2.

Collins, B. G. (1966), Determination of the cosine response of pyranometers, *J. Sci. Instrum.*, *43*, 837–838, doi:10.1088/0950-7671/43/11/416.

Dutton, E. G., J. J. Michalsky, T. Stoffel, B. W. Forgan, J. Hickey, D. W. Nelson, T. L. Alberta, and I. Reda (2001), Measurement of broadband diffuse solar irradiance using current commercial instrumentation with a correction for thermal offset errors, *J. Atmos. Oceanic Technol.*, *18*, 297–314, doi:10.1175/1520-0426(2001)018<0297:MOBDSI>2.0.CO;2.

Fu, Q., and K. N. Liou (1993), Parameterization of the radiative properties of cirrus clouds, *J. Atmos. Sci.*, *50*, 2008–2025, doi:10.1175/1520-0469(1993)050<2008:POTRPO>2.0.CO;2.

Fu, Q., G. Lesins, J. Higgins, and J. J. Michalsky (1999), Aerosol direct radiative forcing: A five year climatology at the ARM SGP CART site, paper presented at Ninth ARM Science Team Meeting, San Antonio, Tex., 22–26 March.

Gulbrandsen, A. (1978), On the use of pyranometers in the study of spectral solar radiation and atmospheric aerosols, *J. Appl. Meteorol.*, *17*, 899–904, doi:10.1175/1520-0450(1978)017<0899:OTUOPI>2.0.CO;2.

Haeffelin, M., S. Kato, A. M. Smith, K. Rutledge, T. Charlock, and J. R. Mahan (2001), Determination of the thermal offset of the Eppley Precision Spectral Pyranometer, *Appl. Opt.*, *40*, 472–484, doi:10.1364/AO.40.000472.

Hansell, R. A., S.-C. Tsay, Q. Ji, N. C. Hsu, M. J. Jeong, S. H. Wang, J. S. Reid, K. N. Liou, and S. C. Ou (2010), An assessment of the surface longwave direct radiative effect of airborne Saharan dust during the NAMMA field campaign, *J. Atmos. Sci.*, *67*, 1048–1065, doi:10.1175/2009JAS3257.1.

Haywood, J., P. Francis, S. Osborne, M. Glew, N. Loeb, E. Highwood, D. Tanré, G. Myhre, P. Formenti, and E. Hirst (2003), Radiative properties and direct radiative effect of Saharan dust measured by the C-130 aircraft during SHADE: 1. Solar spectrum, *J. Geophys. Res.*, *108*(D18), 8577, doi:10.1029/2002JD002687.

International Organization for Standardization (1993), Solar energy—Calibration of a pyranometer using a pyrheliometer, ISO 9846, Geneva, Switzerland.

Ji, Q., and S.-C. Tsay (2000), On the dome effect of Eppley pyrgeometers and pyranometers, *Geophys. Res. Lett.*, *27*, 971–974, doi:10.1029/1999GL011093.

Ji, Q., and S.-C. Tsay (2010), A novel nonintrusive method to resolve the thermal-dome-effect of pyranometers: Instrumentation and observational basis, *J. Geophys. Res.*, *115*, D00K21, doi:10.1029/2009JD013483.

Li, C., et al. (2010), Anthropogenic air pollution observed near dust source regions in northwestern China during springtime 2008, *J. Geophys. Res.*, *115*, D00K22, doi:10.1029/2009JD013659.

Liou, K., Q. Fu, and T. Ackerman (1988), A simple formulation of the delta-four-stream approximation for radiative transfer parameterizations, *J. Atmos. Sci.*, *45*, 1940–1948, doi:10.1175/1520-0469(1988)045<1940:ASFOTD>2.0.CO;2.

McComiskey, A., S. E. Schwartz, B. Schmid, H. Guan, E. R. Lewis, P. Ricchiazzi, and J. A. Ogren (2008), Direct aerosol forcing: Calculation from observables and sensitivities to inputs, *J. Geophys. Res.*, *113*, D09202, doi:10.1029/2007JD009170.

Michalsky, J. J., L. C. Lee, and W. E. Berkheiser, III (1995), Cosine response characteristics of some radiometric and photometric sensors, *Sol. Energy*, *54*(6), 397–402, doi:10.1016/0038-092X(95)00017-L.

Michalsky J. J., et al. (2003), Results from the first ARM diffuse horizontal shortwave irradiance comparison, *J. Geophys. Res.*, *108*(D3), 4108, doi:10.1029/2002JD002825.

Pachauri, R. K., and A. Reisinger (Eds.) (2007), Climate change 2007: Synthesis report, 104 pp., Intergov. Panel on Clim. Change, Geneva, Switzerland. (Available at http://www.ipcc.ch/pdf/assessment-report/ar4/syr/ar4_syr.pdf)

Trenberth, J. E., J. T. Fasullo, and J. Kiehl (2009), Earth's global energy budget, *Bull. Am. Meteorol. Soc.*, *90*, 311–323, doi:10.1175/2008BAMS2634.1.

Walker, J., C. L. Cromer, and J. T. McLean (1991), A technique for improving the calibration of large-area sphere sources, *Proc. SPIE*, *1493*, 224–230, doi:10.1117/12.46707.

Wild, M. (2009), Global dimming and brightening: A review, *J. Geophys. Res.*, *114*, D00D16, doi:10.1029/2008JD011470.

World Meteorological Organization (2008), *Guide to Meteorological Instruments and Methods of Observation*, 7th edition, *WMO-No.8*, Geneva, Switzerland.

J. J. Butler, K. M. Lau, and S.-C. Tsay, Earth Sciences Division, NASA Goddard Space Flight Center, c/o Code 613, College Park, MD 20771, USA.

J. W. Cooper, Sigma Space Corporation, Greenbelt, MD 20706, USA.

R. A. Hansell and Q. Ji, ESSIC, University of Maryland, College Park, MD 20740, USA. (qiang.ji-1@nasa.gov)